Journal of The Electrochemical Society, 2023 **170** 103505

Influence of Induced Local Stress on The Morphology of Porous Anodic Alumina at The Initial Stage of Oxide Growth

Katsiaryna Chernyakova,[1,z] Boriana Tzaneva,[2] Arunas Jagminas,[1] Nikita Lushpa,[3] and Igor Vrublevsky[3]

[1]*State Research Institute Center for Physical Sciences and Technology, LT-10257 Vilnius, Lithuania*
[2]*Technical University of Sofia, 1000 Sofia, Bulgaria*
[3]*Belarussian State University of Informatics and Radioelectronics, 220013 Minsk, Belarus*

A characteristic feature of the disordered pore growth at the initial stage of aluminum anodizing is the development of three large groups of pores: the major pores of larger diameter and two groups of minor pores of smaller diameter. The samples were obtained by the electrochemical oxidation of thin aluminum films (100 nm thick) on SiO_2/Si substrates in a 0.3 M oxalic acid at 30 V at 5 °C–40 °C. According to SEM studies, the pore distribution by diameter for the films obtained at 20 and 40 °C has three distinct peaks at ca. 13.5, 17.2, and 20.3 nm. The ratio of the diameter of major pores to the diameter of minor pores of group 1 or group 2 is constant and approximately equal to 1.17 and 1.51, respectively. The generation of local compressive stress influences the development of porous morphology. The distribution of zones with high and low compressive stress levels inside hexagonal cells is shown, and their correlation with the porous morphology is confirmed. The generation of local stress and strains in the anodic alumina layer with a porous, cellular structure is associated with local areas with changes in the geometric properties on its surface.
 [DOI: 10.1149/1945-7111/ad00dd]

Manuscript submitted August 1, 2023; revised manuscript received September 26, 2023. Published October 16, 2023.

The method of two-stage aluminum anodizing is widely used to obtain films of porous anodic alumina with a highly ordered porous structure.[1–10] According to this, a porous alumina film is obtained in the first stage of the process, and then it is removed using selective etching. After that, a pre-pattern in the form of an array of concave depressions, which are a mirror image of the lower surface of the porous film, remains on the aluminum surface. In the second stage, aluminum anodizing is carried out under the conditions used in the first stage. In this case, the pre-pattern on the aluminum surface with the centers of hexagonally ordered cells serves as a template for forming pores in anodic alumina with a highly ordered structure. Therefore, the first stage of aluminum anodizing is important for forming a hexagonally ordered cellular porous structure of anodic alumina films.[11–15]

The initial stage of forming porous anodic aluminum oxide films is quite well described in the literature.[16–18] In this process of porous film formation, four main stages are distinguished: 1) formation of a barrier-type aluminum oxide layer; 2) initiation of chaotic nucleation of small diameter pores on the surface of the barrier layer; 3) development of individual small diameter pores; and 4) steady-state growth of vertical pore channels with hexagonal packing. Each stage corresponds to a certain segment in the current transients. It should be noted that at the last (fourth) stage, the formation of a system of self-ordered pores with hexagonal packing takes place. However, although the individual stages of the formation of porous films of anodic alumina are well studied, the detailed mechanism of the formation of a porous structure and the transition from the stage of chaotic nucleation of small pores to the formation and development of large pores remains poorly understood.

In addition to the type of electrolyte, its concentration, and the anodizing voltage (U_a), the electrolyte temperature (T_e) significantly affects the anodizing rate and development of an ordered surface.[17,19] A local temperature increase leads to faster chemical dissolution and destruction of the oxide layer, and the temperature difference between the aluminum substrate and the electrolyte is an important parameter influencing the formation of the ordered structure.[2,20,21] Therefore, to better understand the pore formation process at the initial stage of disordered growth, it is necessary to study the peculiarities of developing porous aluminum oxide surface morphology at different electrolyte temperatures.

Experimental

Aluminum films (about 100 nm) were deposited on silicon substrates with a thin silicon dioxide film (SiO_2/Si substrate) by thermal evaporation under a vacuum. From the substrates, square samples with an area of no more than 7.2 cm^2 were cut and anodized in a 0.3 M aqueous solution of oxalic acid at constant $U_a = 30$ V and $T_e = 5$ °C–40 °C until the complete oxidation of aluminum. The anodizing process was carried out in a two-electrode fluoroplastic cell similar to that described by Chernyakova et al.[22] and was controlled by a direct current power supply GW Instek (GPR-30H100). A Viton O-ring set out the anodizing area of ca. 3.14 cm^2. The electrolyte temperature was kept constant using a WK 230 cryostat (Lauda). A platinum grid was used as a cathode. The complete anodizing times decreased twice from 180 to 90 s with increasing T_e from 5 °C to 40 °C.

According to Chernyakova et al.,[22] to provide a more uniform temperature distribution over the surface of the working electrode at different anodizing modes and correspondingly greater pore ordering, we chose a SiO_2/Si substrate because of its higher thermal conductivity (149 W m^{-1} K^{-1}) close to that of aluminum (200 W m^{-1} K^{-1}). The anodizing voltage was also selected according to Chernyakova et al.[22] as, during the oxidation of aluminum thin films in oxalic acid, U_a of 30 V is a turning point at which the mechanism of the formation of porous anodic structure is changed.

Additionally, we formed the samples on high-purity Al foil (99.999%, 250 μm, Alfa Aesar) for the two-stage anodizing experiments and experiments on electropolished Al foil to investigate the peculiarities of the initial growth of the porous anodic alumina on bulk samples with the pre-treated surface. The preliminary preparation operations and the process of the two-stage anodizing of the aluminum foil samples are described by Chernyakova et al.[2] Electropolishing was carried out in $HClO_4$–ethylene glycol–glycerol solution at 5 °C and 17 V dc for 5 min. The first anodizing was conducted in a 0.3 M aqueous oxalic acid solution at 20 °C and 50 V for 30 min. Then, this layer was removed by etching in the mixture of H_3PO_4 and CrO_3 at 75 °C for 2 h. The second anodizing was done under the same conditions. Aluminum was chemically etched in the solution containing $CuCl_2$ and HCl to investigate the reverse side (i.e., anodizing front) of the samples. Then, the alumina layer was

[z]E-mail: katsiaryna.charniakova@ftmc.lt

etched in the mixture of H_3PO_4 and CrO_3 at 75 °C to open pores on the barrier layer side.

The surface morphology of the porous anodic alumina films was studied by scanning electron microscopy (SEM) using a Model Quanta 200 F electron microscope (FEI) with further computer processing of images in the ImageJ software following the data processing procedure described by Chernyakova et al.[22] and Vrublevsky et al.[23] The determination error of pore diameter d_{pore} did not exceed 3.5%. SEM images of the sample surface were processed using the ImageJ software to visualize the structure microrelief and local stress distribution as a color gradient.

Results and Discussion

According to SEM observations, thin anodic alumina films obtained in a 0.3 M aqueous solution of oxalic acid at $U_a = 30$ V and T_e of 15, 20, 30, and 40 °C possess a porous structure (Fig. 1). As seen in Fig. 2, the pore distribution by diameter for the films obtained at T_e of 20 and 40 °C has three distinct peaks at ca. 13.5, 17.2, and 20.3 nm. It is a characteristic of the disordered pore growth at the initial stage of aluminum anodizing, at which three large groups of pores develop.[24]

The larger diameter (D) of 20.3 nm has the major pores in the anodic aluminum oxide film. The two smaller diameters (d_1 and d_2) of 17.2 and 13.5 nm belong to the group of minor pores. From the pore diameter distribution (see Fig. 2, it is also clear that the number of pores for each group is approximately the same. This indicates the location of all pore groups within one unit pore cell in the case of hexagonally ordered pores.

To clearly show how the electrolyte temperature affects the ratio of the diameters of the major and minor pores, we introduced the coefficients K_1 and K_2 equal to the ratio of the diameter of major pores (D) to the diameter of minor pores of group 1 or group 2 (d_1 or d_2)[24] (Table I):

$$K = \frac{D}{d}.$$

As seen from Table I, in the electrolyte temperature range from 5 °C to 40 °C, K_1 and K_2 are constant and approximately equal to 1.17 and 1.51 for the first and second groups of minor pores, respectively. According to Chernyakova et al.,[24] a value of 1.17 for minor pores with a larger diameter is close to the theoretical value equal to $2/\sqrt{3}$. Increasing T_e, the average distribution of the three main pore diameters does not change significantly, but the deviation from these values increases more than twice (from ±0.3 to ±0.7). This shows that the temperature raises the non-uniformity in the pores during the initial stage of anodic layer growth. In addition, the part of larger diameter pores increases (Fig. 2).

The stress arising in the oxide layer in the porous alumina cells during the anodic film growth may affect the development and termination of minor pore growth, as suggested by Chernyakova et al.[24] In this regard, the general pattern of stress distribution in the oxide layer in porous alumina cells was investigated. For such experiments, we used the effect of decreasing the chemical etching rate of the oxide layer in the case of increasing compression stress in the oxide structure.[25–27] Our proposed research scheme includes obtaining porous aluminum oxide with a hexagonally ordered cell structure and then the complete chemical dissolution of the aluminum oxide barrier layer on the aluminum side. The chemical dissolution of the oxide barrier layer stops when the pores are opened, which allows chemical dissolution to be controlled. The

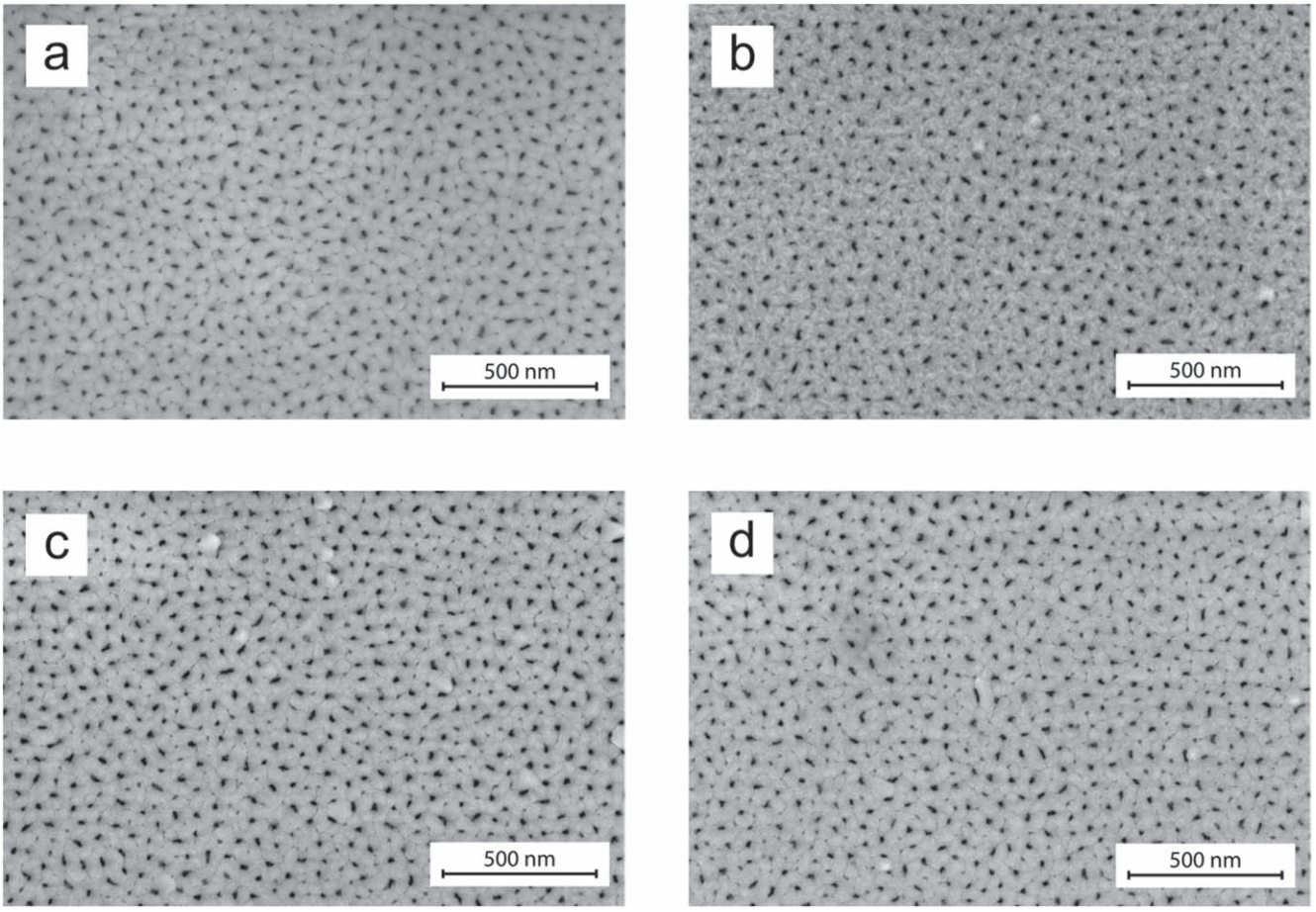

Figure 1. SEM images of surface morphology of porous alumina films on SiO_2/Si substrates obtained in a 0.3 M aqueous solution of oxalic acid at $U_a = 30$ V and T_e of 15 °C (a), 20 °C (b), 30 °C (c), and 40 °C (d).

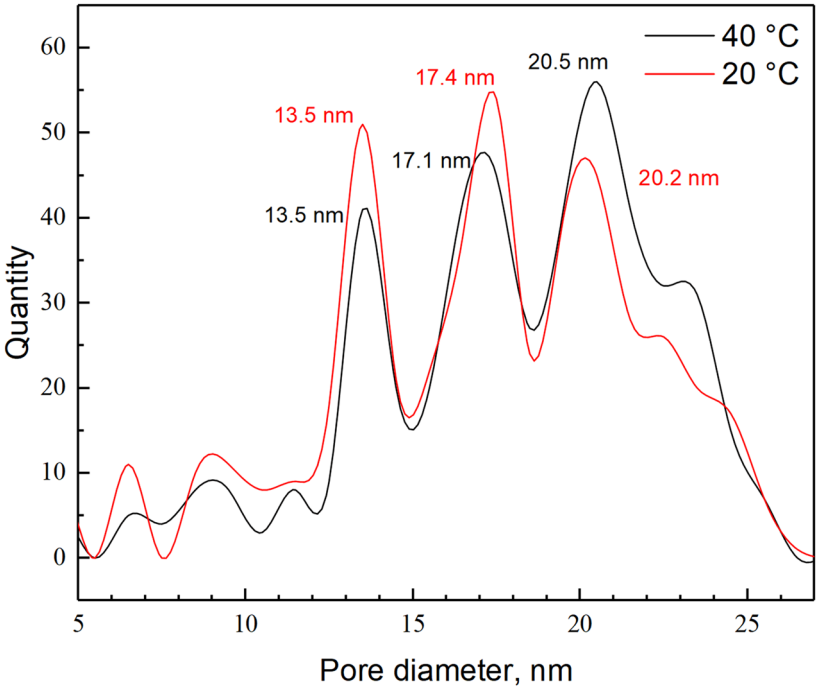

Figure 2. Pore diameter distributions for porous anodic alumina films formed on a SiO_2/Si substrate in a 0.3 M aqueous oxalic acid solution at $U_a = 30$ V and T_e of 20 and 40 °C. These curves were obtained from computer processing of images of the surface of porous anodic films shown in Figs. 1b and 1d, respectively.

Table I. Diameters of the major (D) and two groups of minor pores (d_1 and d_2) and their ratios (K_1 and K_2) for films of porous anodic alumina on SiO_2/Si substrates obtained a 0.3 M aqueous solution of oxalic acid at U_a = 30 V and T_e = 5 °C–40 °C.

T_e, °C	5	15	20	25	30	40
D, nm	20.2 ± 0.2	20.3 ± 0.3	20.2 ± 0.5	20.3 ± 0.7	20,5 ± 0.7	20,5 ± 0.7
d_1, nm	17.2 ± 0.3	17.2 ± 0.4	17.4 ± 0.5	17.3 ± 0.7	17.3 ± 0.7	17.1 ± 0.7
K_1	1.17	1.18	1.18	1.17	1.18	1.18
d_2, nm	13.3 ± 0.3	13.4 ± 0.4	13.5 ± 0.5	13.4 ± 0.7	13.4 ± 0.7	13.5 ± 0.7
K_2	1.52	1.51	1.50	1.51	1.53	1.52

resulting surface, where oxide protrudes (in the higher microrelief areas) corresponding to areas with high levels of compression stress in the oxide layer, will enable us to demonstrate the distribution of zones with high and low levels of compression stress within the hexagonal cells.

Figure 3 shows higher microrelief areas at the triple junction points, characteristic of the resulting relief of the porous aluminum oxide when there are areas with different dissolution rates. This indicates that due to the increased stress level in these areas, there is a decrease in the chemical dissolution rate of anodic alumina. Similar results were obtained earlier.[8,28,29]

As known, the compression stress arises in the oxide layer during aluminum anodizing due to the volume expansion of aluminum oxide.[30–35] Simultaneously, tensile stress occurs in the aluminum layer due to structural deformation. In the Al_2O_3/Al structure, compression stress disappears if aluminum is removed. However, the results shown in Fig. 3 demonstrate that removing the aluminum layer, which is the cause of the structural deformations, did not result in the disappearance of local stress in the alumina. This suggests a different nature of the observed local compression stress.

When studying the stress-strain state in a layer of porous anodic aluminum oxide, it should be considered that local fields of increased stress may occur in some areas.[36] The appearance of such local fields of stress occurs near various inhomogeneities, such as a sharp change in geometric shape, for example, a step on the oxide surface due to pore walls.[37–40] As a rule, the region of increased stress propagation is quite limited, and its dimensions do not exceed a few dimensions of the geometric inhomogeneity region itself.

Thus, the occurrence of fields of local stress and strains in the anodic alumina layer with a porous cellular structure is associated with local areas with changes in the geometric properties on its surface, such as the pore walls. At the pore wall, where the geometric shape changes, the compression stress in the aluminum oxide will be at a maximum. The stress will sharply decrease as we move from this point toward the other pores. Based on this algorithm and the data in Fig. 4, the expected distribution of local stress within each porous cell is schematically illustrated in Fig. 5. For simplicity, the pore area in this figure is excluded from consideration of the stress distribution. The nature of the distribution of local compressive stress outside the pore agrees with the results on the anisotropic etching effect of aluminum oxide.

The distribution of local stress shows that the places with the minimum level of local stress, where incipient pores can develop in the porous cell, are located between each pair of neighboring main pores. From the presented distribution model of local compression stress, it is clear that the preferred place for developing minor pores with the smallest diameter is the boundary between two neighboring cells. However, under real conditions of the aluminum anodizing process, the major pore at the initial stage is dominant. Consequently, the field of local mechanical stresses around it will be the largest. Therefore, the beginning of the development of each minor pore with the smallest diameter will be slightly shifted from this location in the opposite direction to the main pore. The results in Table I show that the distance from the center of the major pore to the center of the minor pore with the smallest diameter is approximately 0.67 R. At the same time, in the ideal case, when simultaneous development of all major pores takes place, this distance is equal to 0.5 R (see Fig. 5).

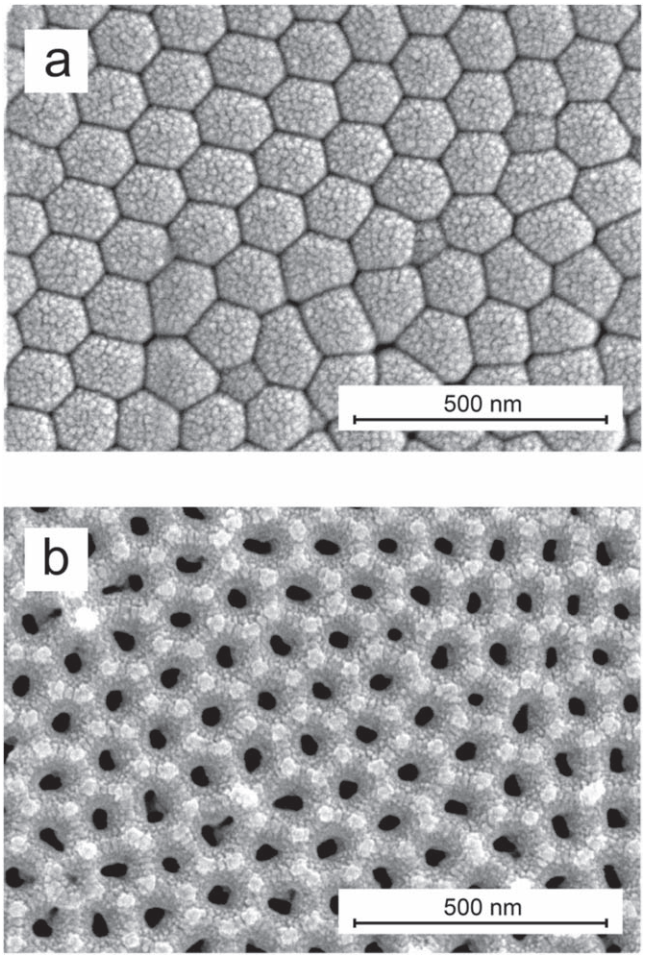

Figure 3. SEM images of the reverse side (i.e., anodizing front) of the porous alumina film obtained in a 0.3 M aqueous solution of oxalic acid at U_a = 50 V (a) and of the surface of this film with pores opened on the barrier layer side (b).

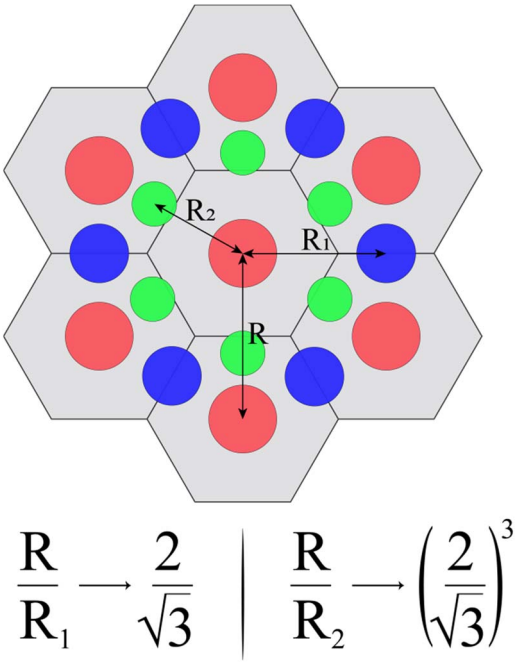

Figure 5. Model for the simultaneous development of the major and minor pores inside an elementary hexagonal cell composed of the major pores.

identical pores with a diameter smaller than the diameter of the major pores stops when the oxide reaches a thickness of about 2–3 diameters of the interpore distance. The reason for this effect is a sharp increase in compressive structural and mechanical stresses in alumina with increasing thickness of individual hexagonal cells due to the growth of the porous anodic film[41–44] and an increase in local compressive stress with increasing pore wall height. The estimation shows that for the porous alumina film formed at 40 V in oxalic acid, the layer with disordered pores has a thickness of about 200–300 nm. This result agrees with the data obtained by Ling[18] and Iwai et al.[45]

As an experimental confirmation of the proposed model, Fig. 6 shows the SEM image of a cross section of the porous anodic

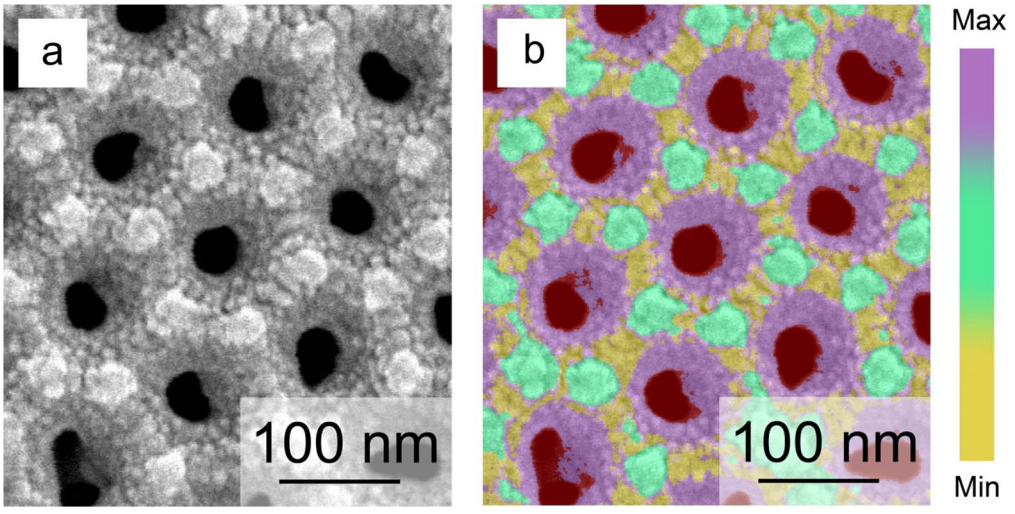

Figure 4. SEM image of the major pores (a) and a model for the distribution of local compression stress within each porous cell (b).

It should also be noted that the growth rate of the minor pores with the smallest diameter will be less than that of the minor pores with a larger diameter and the major pores. Therefore, minor pores with the smallest diameters will be shorter than larger ones. From the presented model, it follows that the development of a group of aluminum oxide film. As can be seen from the figure, minor pores occur only in a thin near-surface layer.

It is of great interest to study and analyze the surface morphology of porous anodic aluminum oxide for an array of pores containing both major and minor pores of smaller diameter. Figure 7 shows the

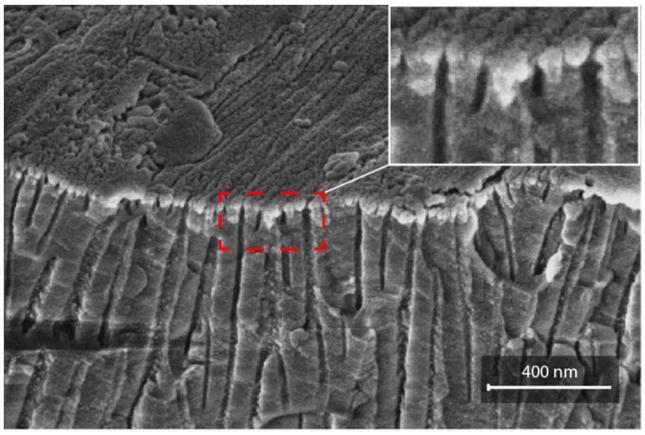

Figure 6. SEM image of a cross section of porous anodic alumina film with major and minor pores near the film surface.

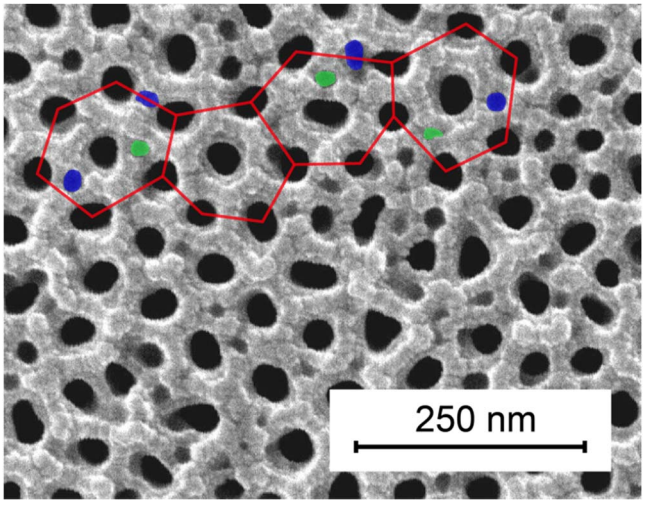

Figure 7. SEM image of the surface morphology of porous anodic alumina film formed in 0.3 M oxalic acid (40 V, 20 °C) on the aluminum foil after its electrochemical polishing. Minor pores (blue pores with a larger diameter and green pores with a smaller diameter) located between two neighboring pores inside the elementary hexagonal cells (red lines) formed by the major pores (black pores).

SEM image of the porous anodic aluminum oxide film surface obtained on aluminum after its electrochemical polishing. The image displays individual minor pores (blue pores with a larger diameter and green pores with a smaller diameter) located between two neighboring pores inside the elementary hexagonal cells (red lines) formed by the major pores (black pores). However, it should be noted that the real porous structure of anodic films can differ significantly from their ideal structure, so the observed deviations of minor pores from the locations predicted by theory may be a consequence of the deviation of the elementary cells composed of the major pores from their ideal hexagonal shape.

It should be noted that the identified patterns of development of minor pores have common features with the peculiarities of the formation of branching pore structures of anodic aluminum oxide. Research on the formation of branching pore structures by reducing anodizing voltage showed that pore branching starts only when the anodizing voltage reaches a certain value. As shown before by Shuoshuo et al.,[46] the possible variants of porous morphology development were studied for the case of four branching pores, including one stem pore, under decreasing voltage. It was found that even when the number of branched pores for each stem pore remains the same, the packing variants of such branched pores can vary. The results showed that the development of three branching pores inside one porous cell has six possible development points, and their combinations have a random character. It means that inside one porous elementary cell formed by a stem pore, six equivalent points can serve as centers for developing new secondary pores while forming a branching porous structure.

Thus, at the initial stage of disordered pore growth during aluminum anodizing, only three large groups of pores develop out of all nucleation centers: major pores and two groups of minor pores, the diameter of which is $2/\sqrt{3}$ and $(2/\sqrt{3})^3$ times less than the diameter of major pores, respectively. The development of two groups of minor pores, smaller in size, is not a random process but occurs in places with the lowest level of local compression stress inside the hexagonal cells formed from the major pores.

Conclusions

The data obtained demonstrate that a characteristic feature of the disordered pore growth at the initial stage of aluminum anodizing is the development of three large groups of pores: the major pores of maximum diameter and two groups of minor pores of smaller diameter. An analysis of the results of pore diameter calculation shows that in the electrolyte temperature range from 5 to 40 °C, the ratio of the diameter of major pores to the diameter of minor pores of group 1 or group 2 is constant and approximately equal to 1.17 and 1.51 for the first and second groups of minor pores, respectively.

The stress arising in the oxide layer in the porous alumina cells during the anodic film growth may affect the development and termination of minor pore growth. In this regard, we investigated the general stress distribution pattern in the oxide layer in porous alumina cells. For such experiments, we used the effect of decreasing the chemical etching rate of the oxide layer in the case of increasing compression stress in the aluminum oxide structure. Our proposed research scheme includes obtaining porous aluminum oxide with a hexagonally ordered cell structure and then the complete chemical dissolution of the aluminum oxide barrier layer on the aluminum side.

Our results indicate that generating local stress and strains in the anodic alumina layer with a porous, cellular structure is associated with local areas with changes in the geometric properties on its surface, such as the pore walls. At the pore wall, where the geometric shape changes, the compression stress in the aluminum oxide will be at a maximum. The stress will sharply decrease as we move from this point toward the other pores. The increase in compressive stress in the anodic alumina during aluminum anodizing leads to an interruption in the development of two groups of minor pores.

Acknowledgments

This work was supported by the Belarusian Republican Foundation for Fundamental Research [Grant No B22KI-044].

ORCID

Katsiaryna Chernyakova https://orcid.org/0000-0002-6616-4353
Boriana Tzaneva https://orcid.org/0000-0002-3289-9124
Arunas Jagminas https://orcid.org/0000-0003-0191-8588
Igor Vrublevsky https://orcid.org/0000-0002-6796-8994

References

1. R. Kondo, T. Kikuchi, S. Natsui, and R. O. Suzuki, *Mater. Lett.*, **183**, 285 (2016).
2. K. Chernyakova, B. Tzaneva, I. Vrublevsky, and V. Videkov, *J. Electrochem. Soc.*, **167**, 103506 (2020).
3. L. Zaraska, W. J. Stępniowski, E. Ciepiela, and G. D. Sulka, *Thin Solid Films*, **534**, 155 (2013).
4. T. Kikuchi, F. Onoda, M. Iwai, and R. O. Suzuki, *Appl. Surf. Sci.*, **546**, 149090 (2021).
5. L. Zaraska, W. J. Stępniowski, G. D. Sulka, E. Ciepiela, and M. Jaskuła, *Appl. Phys. A Mater. Sci. Process.*, **114**, 571 (2014).
6. Y. Sato, H. Asoh, and S. Ono, *Mater. Trans.*, **54**, 1993 (2013).

7. L. Zaraska, W. J. Stępniowski, M. Jaskuła, and G. D. Sulka, *Appl. Surf. Sci.*, **305**, 650 (2014).
8. M. Pashchanka, *Nanomaterials*, **11**, 2271 (2021).
9. A. Ruiz-Clavijo, O. Caballero-Calero, and M. Martín-González, *Nanoscale*, **13**, 2227 (2021).
10. M. Mohajeri and H. Akbarpour, *J. Electroanal. Chem.*, **705**, 57 (2013).
11. H. Masuda, H. Yamada, M. Satoh, H. Asoh, M. Nakao, and T. Tamamura, *Appl. Phys. Lett.*, **71**, 2770 (1997).
12. J. Choi, Y. Luo, R. B. Wehrspohn, R. Hillebrand, J. Schilling, and U. Gösele, *J. Appl. Phys.*, **94**, 4757 (2003).
13. H. Masuda and K. Fukuda, *Science*, **268**, 1466 (1995).
14. W. J. Stepniowski, M. Michalska-Domańska, M. Norek, E. Twardosz, W. Florkiewicz, W. Polkowski, D. Zasada, and Z. Bojar, *Surf. Coatings Technol.*, **258**, 268 (2014).
15. F. Le Coz, L. Arurault, and L. Datas, *Mater. Charact.*, **61**, 283 (2010).
16. G. E. Thompson, *Thin Solid Films*, **897**, 192 (1997).
17. W. Lee and S. J. Park, *Chem. Rev.*, **114**, 7487 (2014).
18. Z. Ling and Y. Li, *Nanoporous Alumina*, ed. D. Losic and A. Santos (Berlin) (Springer, Cham)p. 1 (2015).
19. O. Jessensky, F. Müller, and U. Gösele, *J. Electrochem. Soc.*, **145**, 3735 (1998).
20. I. De Graeve, H. Terryn, and G. E. Thompson, *J. Appl. Electrochem.*, **32**, 73 (2002).
21. F. A. Bruera, G. R. Kramer, M. L. Vera, and A. E. Ares, *Surfaces and Interfaces*, **18**, 100448 (2020).
22. K. Chernyakova, I. Vrublevsky, V. Klimas, and A. Jagminas, *J. Electrochem. Soc.*, **165**, E289 (2018).
23. I. Vrublevsky, A. Ispas, K. Chernyakova, and A. Bund, *J. Solid State Electrochem.*, **20**, 2765 (2016).
24. K. Chernyakova, V. Klimas, A. Jagminas, N. Lushpa, I. Vrublevsky, and S. Jankauskas, *Electrochem. Commun.*, **143**, 107391 (2022).
25. V. Sergo, O. Sbaizero, and D. R. Clarke, *Biomaterials*, **18**, 477 (1997).
26. J. A. Nychka, D. Li, and B. Alexander, *J. Mech. Behav. Biomed. Mater.*, **1**, 243 (2008).
27. D. Palamara, J. E. A. Palamara, M. J. Tyas, M. Pintado, and H. H. Messer, *Dent. Mater.*, **17**, 109 (2001).
28. M. Norek, *J. Electrochem. Soc.*, **169**, 123503 (2022).
29. M. Pashchanka and J. J. Schneider, *Phys. Chem. Chem. Phys.*, **18**, 6946 (2016).
30. Ö. Ö. Çapraz, P. Shrotriya, P. Skeldon, G. E. Thompson, and K. R. Hebert, *Electrochim. Acta*, **159**, 16 (2015).
31. O. Jessensky, F. Müller, and U. Gösele, *Appl. Phys. Lett.*, **72**, 1173 (1998).
32. L. Arurault, *Trans. Inst. Met. Finish.*, **86**, 51 (2008).
33. G. Knörnschild, A. A. Poznyak, A. G. Karoza, and A. Mozalev, *Surf. Coatings Technol.*, **275**, 17 (2015).
34. I. Vrublevsky, V. Parkoun, V. Sokol, J. Schreckenbach, and G. Marx, *Appl. Surf. Sci.*, **222**, 215 (2004).
35. I. Vrublevsky, V. Parkoun, J. Schreckenbach, and G. Marx, *Appl. Surf. Sci.*, **220**, 51 (2003).
36. J. Liao, Z. Ling, Y. Li, and X. Hu, *ACS Appl. Mater. Interfaces*, **8**, 8017 (2016).
37. S. Mader, *J. Electron. Mater.*, **9**, 963 (1980).
38. I. A. Blech and E. S. Meieran, *J. Appl. Phys.*, **38**, 2913 (1967).
39. S. Isomae, *J. Appl. Phys.*, **52**, 2782 (1981).
40. R. Zeyfang, *Solid State Electron.*, **14**, 1035 (1971).
41. Ö. Ö. Çapraz, P. Shrotriya, P. Skeldon, G. E. Thompson, and K. R. Hebert, *Electrochim. Acta*, **167**, 404 (2015).
42. K. Chernyakova, I. Vrublevsky, A. Jagminas, and V. Klimas, *J. Solid State Electrochem.*, **25**, 1453 (2021).
43. K. R. Hebert and P. Mishra, *J. Electrochem. Soc.*, **165**, E737 (2018).
44. K. R. Hebert and P. Mishra, *J. Electrochem. Soc.*, **165**, E744 (2018).
45. M. Iwai, T. Kikuchi, and R. O. Suzuki, *ECS J. Solid State Sci. Technol.*, **9**, 044004 (2020).
46. C. Shuoshuo, L. Zhiyuan, H. Xing, and L. Yi, *J. Mater. Chem.*, **19**, 5717 (2009).